Mycobacterium tuberculosis β-Ketoacyl-Acyl Carrier Protein (ACP) Reductase: Kinetic and Chemical Mechanisms†

Rafael G. Silva,‡,§ Luiz Pedro S. de Carvalho,‡,|| John S. Blanchard,⊥ Diógenes S. Santos,*,‡ and Luiz A. Basso*,‡

Centro de Pesquisas em Biologia Molecular e Funcional, Faculdade de Biociências e Faculdade de Farmácia, Instituto de Pesquisas Biomédicas, PUCRS, 6681/92-A Avenida Ipiranga, 90619-900, Porto Alegre, RS, Brazil, Programa de Pós-graduação em Ciências Biológicas: Bioquímica, Instituto de Ciências Básicas da Saúde, Universidade Federal do Rio Grande do Sul (UFRGS), Porto Alegre, RS, Brazil, and Department of Biochemistry, Albert Einstein College of Medicine, 1300 Morris Park Avenue, Bronx, New York 10461

Received June 6, 2006; Revised Manuscript Received August 11, 2006

ABSTRACT: β-ketoacyl-acyl carrier protein (ACP) reductase from *Mycobacterium tuberculosis* (MabA) is responsible for the second step of the type-II fatty acid elongation system of bacteria, plants, and apicomplexan organisms, catalyzing the NADPH-dependent reduction of β-ketoacyl-ACP to generate β-hydroxyacyl-ACP and $NADP^+$. In the present work, the *mabA*-encoded MabA has been cloned, expressed, and purified to homogeneity. Initial velocity studies, product inhibition, and primary deuterium kinetic isotope effects suggested a steady-state random bi-bi kinetic mechanism for the MabA-catalyzed reaction. The magnitudes of the primary deuterium kinetic isotope effect indicated that the C_4-*proS* hydrogen is transferred from the pyridine nucleotide and that this transfer contributes modestly to the rate-limiting step of the reaction. The pH-rate profiles demonstrated groups with p*K* values of 6.9 and 8.0, important for binding of NADPH, and with p*K* values of 8.8 and 9.6, important for binding of AcAcCoA and for catalysis, respectively. Temperature studies were employed to determine the activation energy of the reaction. Solvent kinetic isotope effects and proton inventory analysis established that a single proton is transferred in a partially rate-limiting step and that the mechanism of carbonyl reduction is probably concerted. The observation of an inverse $^{D_2O}V/K$ and an increase in ^{D_2O}V when [4*S*-^{2}H]NADPH was the varied substrate obscured the distinction between stepwise and concerted mechanisms; however, the latter was further supported by the pH dependence of the primary deuterium kinetic isotope effect. Kinetic and chemical mechanisms for the MabA-catalyzed reaction are proposed on the basis of the experimental data.

Tuberculosis (TB),[1] an infectious disease caused by the Gram-positive bacillus *Mycobacterium tuberculosis*, is a major human health threat, with an annual rate of 8.8 million new cases and 1.7 million deaths, 95% of which occur in developing countries (*1*). The treatment of TB demands a standard 6 month administration of several drugs, whose side effects lead to patient noncompliance (*2*). In addition, there is an increasing incidence of infection with multidrug-resistant tuberculosis strains (MDR-TB), defined as being resistant to at least two drugs commonly used to treat TB, isoniazid and rifampicin (*3*). There is thus an urgent need for the development of new antimycobacterial agents, and the detailed molecular characterization of new targets is a step of paramount importance toward this goal.

The type-II fatty acid elongation system (FAS II) of bacteria, in which the reactions are catalyzed by different enzymes, each encoded by a discrete gene, constitutes an attractive target for inhibition, because it contrasts with the type-I fatty acid elongation system (FAS I) of mammals, whose reactions are catalyzed by a single, multifunctional polypeptide (*4*). *M. tuberculosis* possesses both systems. FAS I is responsible for the biosynthesis of acyl chains with 14−16 carbons, while FAS II generates fatty acids with 25−56 carbons. The two systems provide precursors for the biosynthesis of mycolic acids, which contain very long-chain fatty acids that are prominent and essential components of the mycobacterial cell wall (*5*). The FAS II system of mycobacteria elongates fatty acids by adding C2 units to the

† This work was supported by Millennium Initiative Program MCT-CNPq, Ministry of Health/DECIT−Secretary of Health Policy, and PRONEX/FAPERGS/CNPq (Brazil) to D.S.S. and L.A.B. and NIH Grant AI33696 to J.S.B. D.S.S. (304051/1975-06) and L.A.B. (520182/99-5) are Research Career Awardees from the National Research Council of Brazil (CNPq). R.G.S. is a predoctoral fellow from CNPq.

* To whom correspondence should be addressed: Telephone/Fax: +55-51-33203629. E-mail: luiz.basso@pucrs.br (L.A.B.); diogenes@pucrs.br (D.S.S.).

‡ Instituto de Pesquisas Biomédicas.

§ Instituto de Ciências Básicas da Saúde.

|| Current address: Department of Biochemistry, Albert Einstein College of Medicine, 1300 Morris Park Avenue, Bronx, NY 10461.

⊥ Albert Einstein College of Medicine.

[1] Abbreviations: TB, tuberculosis; MDR-TB, multidrug-resistant tuberculosis; FAS II, type-II fatty acid elongation system; FAS I, type-I fatty acid elongation system; ACP, acyl carrier protein; MabA, β-ketoacyl-ACP reductase from *M. tuberculosis*, FabG, β-ketoacyl-ACP reductase from other organisms; SDR, short-chain dehydrogenases/reductases; AcAcCoA, acetoacetyl-coenzyme A; β-HBCoA, β-hydroxyacetyl-coenzyme A, IPTG, isopropyl-1-thio-β-D-galactopyranoside; NADPD, deuterated pyridine nucleotide; ESI−MS, electronspray ionization mass spectrometry; InhA, 2-*trans*-enoyl-ACP reductase from *M. tuberculosis*.

10.1021/bi0611210 CCC: $33.50
Published on Web 10/07/2006

Scheme 1: β-Ketoacyl-ACP-Reductase-Catalyzed Reaction

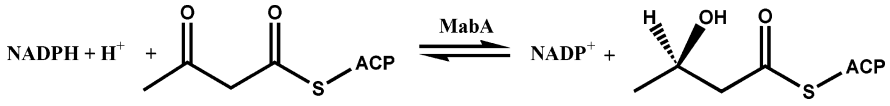

final product of FAS I, through four cyclical enzyme-catalyzed reactions, namely, a condensation, a carbonyl reduction, a dehydration, and an enoyl reduction. The cycle proceeds until a saturated fatty acid of appropriate length is reached. In all of the steps, the growing acyl chain is attached to the acyl carrier protein (ACP) (*4*, *5*).

The second step of this elongation cycle is the NADPH-dependent reduction of β-ketoacyl-ACP (Scheme 1), catalyzed by the *mabA*-encoded β-ketoacyl-ACP reductase from *M. tuberculosis* (MabA) (*6*). The enzyme from *M. tuberculosis* shows a strong preference for NADPH over NADH and is more active with long β-ketoacyl chains (*7*). MabA belongs to the family of short-chain dehydrogenases/reductases (SDR) (*8*), and its crystal structure revealed a conserved Rossman fold and the Ser-Tyr-Lys catalytic triad conserved among SDR members (*9*). Furthermore, MabA has been shown to be a target of isoniazid, one of the main drugs used in the treatment of TB (*10*).

Here, the cloning and expression of the *M. tuberculosis mabA* gene and the purification of the reductase are reported. Initial velocity studies, product inhibition, primary, solvent, and multiple isotope effects, temperature effects, and the pH dependence of the kinetic parameters and isotope effects have been employed to investigate the kinetic and chemical mechanisms of the MabA-catalyzed reaction using acetoacetyl-coenzyme A (AcAcCoA) as a substrate. The analysis of the experimental data suggests a steady-state random kinetic mechanism and a chemical mechanism in which hydride transfer and alkoxide protonation occur in the same step. The results described here could be useful in developing new inhibitors of MabA enzyme activity with potential antitubercular activity.

EXPERIMENTAL PROCEDURES

Materials. All chemicals were of analytical or reagent grade and were used without further purification unless stated otherwise. NADPH, $NADP^+$, AcAcCoA, β-hydroxybutyryl-CoA (β-HBCoA), ATP, *Leuconostoc mesenteroides* glucose-6-phosphate dehydrogenase (type XXIII), and yeast hexokinase (type C-300) were from Sigma. Deuterium oxide (99.9 atom % D) was from Cambridge Isotope Laboratories, and D-glucose-1-*d* (97 atom % D) was from Aldrich. Restriction enzymes and T4 DNA ligase were from Invitrogen.

Cloning, Expression, and Purification of MabA. The *M. tuberculosis mabA* gene was polymerase chain reaction (PCR)-amplified from the plasmid pET-3d::*mabA*[2] to generate a blunt-ended DNA fragment harboring *Nde*I and *Hin*dIII restriction sites. The oligonucleotide primer sequences were 5′-ATTCATATGACTGCCACAGCCACTGA-AGG-3′ (forward) and 5′-TAAGCTTTCAGTCGCCCATACCCATGCC-3′ (reverse). The DNA fragment was amplified with *Pfu* DNA polymerase (Stratagene), ligated into the pCR-blunt plasmid, and transformed into One Shot TOP10 cells according to the instructions of the manufacturer (Invitrogen). Plasmid DNA recovered from these cells was digested with *Nde*I and *Hin*dIII, and the isolated insert was ligated into the pET-23a(+) expression plasmid (Novagen), previously treated with the same enzymes. The plasmid was then transformed into *Escherichia coli* BL21(DE3) cells (Novagen). DNA sequence analysis showed that no mutations were introduced in the cloned *mabA* gene by the PCR amplification step. *E. coli* BL21(DE3) cells containing the recombinant plasmid were grown in Luria−Bertani medium containing 50 μg mL^{-1} carbenicillin, at 37 °C to an $A_{600\ nm}$ of 0.4, and induced by the addition of isopropyl-1-thio-β-D-galactopyranoside (IPTG) to a final concentration of 0.1 mM. Cells were allowed to grow for an additional 4 h and harvested by centrifugation at 20800*g* for 30 min. Cells were resuspended in 20 mM NaH_2PO_4 at pH 7.0 containing 10 mM NaCl (buffer A), incubated with 0.2 mg mL^{-1} lysozyme, disrupted by sonication, and centrifuged at 48000*g* for 60 min to remove cell debris. The supernatant was loaded on an FPLC Q-Sepharose Fast Flow column (Amersham Pharmacia Biotech), pre-equilibrated with the same buffer. The column was washed with 10 column volumes of buffer A, and the adsorbed material was eluted with a linear gradient (0−100%) of 20 column volumes of 20 mM NaH_2PO_4 at pH 7.0 containing 0.5 M NaCl (buffer B). The fractions containing MabA were pooled, concentrated using an Amicon ultrafiltration membrane [molecular weight cutoff (MWCO) of 10 000 Da], and loaded onto a Sephacryl S-200 column (GE Healthcare) pre-equilibrated with buffer A. The column was eluted with buffer A, and the fractions containing MabA were pooled and stored at −20 °C. The protein content was analyzed by sodium dodecyl sulfate−polyacrylamide gel electrophoresis (SDS−PAGE) (*11*). The protein concentration was determined by the method of Bradford et al. (*12*), using the Bio-Rad protein assay kit (Bio-Rad) and bovine serum albumin as the standard. The enzyme was further biophysically characterized by electrospray ionization mass spectrometry (ESI−MS), N-terminal sequence, and ultracentrifugation analysis.

Synthesis of [4S-^{2}H]NADPH. [4S-^{2}H]NADPH was synthesized according to the method of Ottolina et al. (*13*) and purified on a Mono-Q anion-exchange column (GE Healthcare) as previously described (*14*). The fractions with $A_{260\ nm}/A_{340\ nm} \leq 2.3$ were pooled.

Enzymatic Assay for MabA. All assays were performed under initial rate conditions at 25 °C and 100 mM *N*-2-hydroxyethylpiperazine-*N*′-2-ethanesulfonic acid (HEPES) at pH(D) 7.0, unless stated otherwise. The oxidation of NADPH, in the presence of AcAcCoA and MabA, was monitored spectrophotometrically at either 340 nm ($\epsilon = 6220\ M^{-1}\ cm^{-1}$) or 370 nm ($\epsilon = 2320\ M^{-1}\ cm^{-1}$).

Initial Velocity and Product Inhibition Patterns. To determine the kinetic constants and initial velocity patterns, MabA activity was measured in the presence of variable concentrations of one substrate and several fixed concentrations of the other. Product inhibition patterns were deter-

[2] A kind gift from Dr. William Jacobs, Jr. (Albert Einstein College of Medicine, New York).

mined by measuring initial rates at variable concentrations of one substrate, fixed subsaturating concentration of the cosubstrate, and fixed levels of product (either $NADP^+$ or β-HBCoA).

pH-Rate Profiles. The pH dependence of the kinetic parameters was determined by measuring initial velocities in the presence of varying concentrations of one substrate and a saturating level of the other, at different pH values in the following buffers: piperazine-1,4-bis(2-ethanesulfonic acid) (PIPES) (pH 5.8−6.0), HEPES (pH 6.5−8.5), and boric acid (pH 9.0−10). Before performing this experiment, the enzyme had been incubated at the pH values cited above and assayed under standard conditions to ensure enzyme stability at the tested pH range. In control experiments, appropriate overlaps were performed to rule out buffer effects on the enzyme activity. The pH profile studies have identified a pH region where the kinetic parameters are pH-independent, allowing for the determination of solvent kinetic isotope effects.

Energy of Activation. To determine the energy of activation of the MabA-catalyzed reaction, initial velocities were measured in the presence of varying concentrations of one substrate and a saturating level of the other, at temperatures ranging from 15 to 37 °C. MabA was incubated for several minutes in all of the temperatures tested and assayed under standard conditions to ensure enzyme stability under all conditions.

Kinetic Isotope Effects and Proton Inventory. For all isotope effect experiments, commercial NADPH was further purified on a Mono-Q column. Primary deuterium kinetic isotope effects were determined by measuring initial rates in the presence of varying concentrations of one substrate and several fixed concentrations of the other, using [4*S*-4-^{1}H]- or [4*S*-4-^{2}H]-NADPH. Solvent kinetic isotope effects were determined by measuring initial velocities using a saturating level of one substrate and varying concentrations of the other in either H_2O or 90 atom % D_2O. The proton inventory was determined using saturating concentrations of both substrates at various mole fractions of D_2O. Multiple kinetic isotope effects were measured by determining the solvent isotope effects using the deuterated pyridine nucleotide (NADPD) as the varied substrate. Each individual initial rate datum is the average of duplicate or triplicate measurements. The notation utilized to express isotope effects is that of Northrop (*15*) as extended by Cook and Cleland (*16*).

Assignment of the Regiospecificity of Hydride Transfer. To probe the regiospecificity of the hydride transfer catalyzed by MabA, we reduced the acetoacetyl-CoA substrate with either NADPH or [4*S*-4^{2}H]-NADPH and determined the site of incorporation by ^{1}H nuclear magnetic resonance (NMR) spectroscopy. To drive the reaction to completion and facilitate the purification of the hydroxy acyl-CoA product, we used a low concentration of $NADP^+$ and a regenerating system that synthesizes NADPL by the action of glucose dehydrogenase from *Thermoplasma acidophilum*, EC 1.1.1.47 (Sigma), and either ^{1}H- or ^{2}H-β-D-glucose. Typical reaction mixtures contained 20 mM sodium phosphate buffer at pH 7.0, 2.5 mM AcAcCoA, 100 μM $NADP^+$, 30 mM ^{1}H- or ^{2}H-β-D-glucose, 16 units of glucose dehydrogenase, and 1 μM MabA in 1000 μL. Reactions were incubated at 37 °C for 2 h, and proteins were removed by filtration on a 10 kDa cutoff Microcon filter (Millipore) and frozen until purification. Purification of β-hydroxybutyryl-CoA was performed using a Mono-Q column. Fractions containing the product were pooled together and lyophilized. Prior to analysis by NMR, samples were suspended in 1200 μL of D_2O, filtered, and kept at 4 °C. Proton NMR spectra were recorded at 25 °C at 300 MHz with a Bruker DXR300 spectrometer (AECOM−Structural NMR Resource), averaging 128 scans. Water suppression was used to minimize the signal of the water molecules.

Data Analysis. Values of the kinetic parameters and their standard errors were obtained by fitting the data to the appropriate equations by using the nonlinear regression function of SigmaPlot 2000 (SPSS, Inc.). Initial rate data at a single concentration of the fixed substrate were fitted to eq 1.

$$v = VA/(K + A) \quad (1)$$

The data for intersecting initial velocity patterns were fitted to eq 2, describing a sequential mechanism.

$$v = VAB/(K_{ia}K_b + K_aB + K_bA + AB) \quad (2)$$

Noncompetitive inhibition data were fitted to eq 3.

$$v = VA/[K(1 + I/K_{is}) + A(1 + I/K_{ii})] \quad (3)$$

For eqs 1−3, V is the maximal velocity, A and B are substrate concentrations, I is the inhibitor concentration, K_{ia} is the dissociation constant for A, K_a and K_b are Michaelis constants for substrates A and B, respectively, and K_{is} and K_{ii} are the slope and intercept inhibition constants, respectively.

All pH profiles were fitted to eqs 4 or 5, where y is the kinetic parameter, C is the pH-independent value of y, H is the proton concentration, and K_a and K_b are, respectively, the apparent acid and base dissociation constants for ionizing groups.

$$\log y = \log[C/(1 + K_b/H)] \quad (4)$$

$$\log y = \log[C/(1 + H/K_a + K_b/H)] \quad (5)$$

The data for temperature effects were fitted to eq 6, where k is the maximal reaction rate, E_a is the energy of activation, T is the temperature in Kelvin, R is the gas constant (1.98 cal mol^{-1}), and A is a pre-exponential factor that correlates collision frequency and the probability of the reaction occurring when reactant molecules collide.

$$\log k = (-E_a/2.3R)(1/T) + \log(A) \quad (6)$$

Isotope effect data were fitted to eqs 7 or 8, which assume isotope effects on both V/K and V and on V only, respectively. In these equations, $E_{V/K}$ and E_V are the isotope effects minus 1 on V/K and V, respectively, and F_i is the fraction of deuterium label in the substrate.

$$v = VA/[K(1 + F_iE_{V/K}) + A(1 + F_iE_V)] \quad (7)$$

$$v = VA/[K + A(1 + F_iE_V)] \quad (8)$$

RESULTS AND DISCUSSION

Cloning, Expression, Purification, and Biophysical Characterization of MabA. The PCR-amplified fragment of the

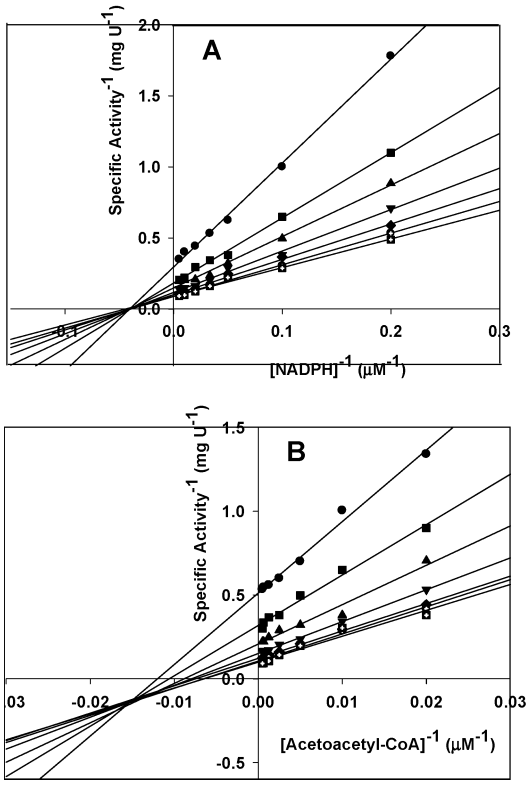

FIGURE 1: Intersecting initial velocity patterns for MabA with either NADPH (A) or AcAcCoA (B) as the variable substrate. Each curve represents varied−fixed levels of the cosubstrate. One unit of MabA is the amount of enzyme that catalyzes the oxidation of 1 μmol of NADPH per minute in a 1 cm optical path.

expected length was cloned into the expression vector pET-23a(+) and shown to be the *mabA* gene from *M. tuberculosis* by sequence analysis, which also confirmed that no mutations were introduced by the PCR amplification step. Maximal expression of recombinant MabA was achieved 4 h after induction with 0.1 mM IPTG. MabA was successfully purified to homogeneity, in an active form, by a two-step purification protocol, and a single band of the expected molecular weight was observed by SDS−PAGE. A total of 10 mg of pure protein was obtained from 4.5 g of cell paste. The present protocol is significantly different from one previously reported (*7*), because this enzyme is not His-tagged. ESI−MS analysis demonstrated that the recombinant enzyme has a subunit molecular weight of 25 563 Da. The predicted molecular weight based on its amino acid sequence is 25 697 Da, while the predicted molecular weight with the first methionine removed is 25 566 Da, and N-terminal amino acid sequence analysis confirmed that the initiator methionine had been completely removed. Analytical ultracentrifugation analysis suggested that the enzyme, at a concentration of 8 μM, was present as a dimer in solution. This is in agreement with the previously described dimer−tetramer equilibrium for MabA, with a dissociation constant of 22 μM (*7*).

Initial Velocity Patterns and Kinetic Parameters. To distinguish between a sequential and a ping-pong mechanism, initial velocity patterns were determined using either AcAcCoA or NADPH as the variable substrate. Analysis of the double-reciprocal plots showed intersecting patterns for both substrates (Figure 1), consistent with ternary complex formation and a sequential mechanism. Because the double-reciprocal plots intersect to the left of the *y* axis, a rapid equilibrium ordered mechanism was ruled out. Similar intersecting initial velocity patterns have been reported for *Streptococcus pneumoniae* β-ketoacyl-ACP reductase (FabG) (*17*), and for the 2-*trans*-enoyl-ACP reductase from *M. tuberculosis* (InhA) (*18*) and *Brassica napus* (*19*), which exhibit structural similarities with MabA. Fitting the data to eq 2 yielded values of $k_{cat} = 7 \pm 0.5$ s^{-1}, $K_{NADPH} = 26 \pm 3$ μM, $K_{AcAcCoA} = 165 \pm 19$ μM, $k_{cat}/K_{NADPH} = 2.69 \times 10^5$ M^{-1} s^{-1}, and $k_{cat}/K_{AcAcCoA} = 4.24 \times 10^4$ M^{-1} s^{-1}. The k_{cat} value obtained in the present study is 3-fold larger, and $K_{AcAcCoA}$ is 9-fold lower compared to previously reported kinetic parameter values for this enzyme, obtained using 100 mM phosphate buffer (*7*). We have observed the inhibition of MabA activity when assays were performed in 100 mM phosphate buffer instead of HEPES (data not shown), which may account for the differences observed.

Table 1: Product Inhibition Patterns for *M. tuberculosis* β-Ketoacyl-ACP Reductase

varied substrate	product inhibitor	inhibition type[a]	K_{is} (μM)[b]	K_{ii} (μM)[c]
NADPH	NADP$^+$	NC	7 ± 2	11 ± 3
AcAcCoA	NADP$^+$	NC	13 ± 2	23 ± 5
NADPH	β-HBCoA	NC	26 ± 6	130 ± 21
AcAcCoA	β-HBCoA	NC	20 ± 3	42 ± 9

[a] NC = noncompetitive. [b] K_{is} is the slope inhibition constant. [c] K_{ii} is the intercept inhibition constant.

Product Inhibition Patterns. To gather information about the order of addition of substrates, both NADP$^+$ and β-HBCoA were utilized in product inhibition studies (Table 1). The data were best-fitted to the equation describing noncompetitive inhibition against both substrates, with the family of double-reciprocal plots intersecting above the *x* axis. This is compatible with a steady-state random bi-bi kinetic mechanism (*20*). These results are different from the ordered mechanisms reported for the *B. napus* enoyl-ACP reductase (*19*) and *Plasmodium falciparum* FabG (*21*). An ordered mechanism was also suggested for the *E. coli* FabG based on structural data, although both substrates were able to independently bind to the enzyme (*22*). However, a random bi-bi mechanism was recently reported for the *S. pneumoniae* FabG, on the basis of product inhibition and isotope effects, with substrate binding and dissociation suggested to be in rapid equilibrium (*17*).

Primary Kinetic Isotope Effects. To probe for rate-limiting steps and determine the stereospecificity of hydride transfer, primary deuterium kinetic isotope effects were determined (Table 2). From the magnitude of these isotope effects, it is possible to conclude that MabA catalyzes the transfer of the C_4-*proS* hydrogen from NADPH to the β-ketoacyl-ACP-(CoA) substrate. The same stereospecifictity was found for *S. pneumoniae* FabG (*17*) and *M. tuberculosis* enoyl-ACP reductase (*18*). Isotope effects on *V* report on events following the formation of the ternary complex capable of undergoing catalysis, which include the chemical steps, possible enzyme conformational changes, and product release. Isotope effects on *V*/*K* report on steps in the reaction mechanism from the binding of the isotopically labeled substrate to the first irreversible step, usually considered to be the release of the first product (*15*). The apparent classical limit for primary deuterium kinetic isotope effects on the maximal velocity is around 8, although, in a less rigorous

Table 2: Kinetic Isotope Effects for *M. tuberculosis* β-Ketoacyl-ACP Reductase

parameter	pH(D)	isotope effect[a]
$^{D}V/K_{AcAcCoA}$	7.0	1.6 ± 0.08
$^{D}V_{AcAcCoA}$	7.0	1.5 ± 0.01
$^{D}V/K_{NADPH}$	7.0	2.5 ± 0.09
$^{D}V_{NADPH}$	7.0	1.4 ± 0.02
$^{D_2O}V/K_{AcAcCoA}$	7.0	1.0 ± 0.10
$^{D_2O}V_{AcAcCoA}$	7.0	2.3 ± 0.07
$^{D_2O}V/K_{NADPH}$	7.0	1.3 ± 0.02
$^{D_2O}V_{NADPH}$	7.0	2.4 ± 0.06
$^{D_2O}V/K_{[4S-^2H]NADPH}$	7.0	0.58 ± 0.04
$^{D_2O}V_{[4S-^2H]NADPH}$	7.0	2.3 ± 0.10
$^{D}V/K_{NADPH}$	10.0	2.5 ± 0.11
$^{D}V_{NADPH}$	10.0	2.4 ± 0.09

[a] Value ± standard error obtained upon fitting the data to the appropriate equations.

practice, values as low as 2 have sometimes been accepted as evidence of a rate-determining step (*15*). The ^{D}V values obtained for MabA using either AcAcCoA (1.5) or NADPH (1.4) as the variable substrate indicate that hydride transfer is only partly rate-limiting, because they are relatively small even if compared to the lower limit of 2. The values for primary deuterium isotope effects of biochemical interest usually range from 3 to 7 (*23*), and steps such as conformational changes accompanying hydride transfer and product release may account for the lower values. In particular, primary deuterium kinetic isotope effects typically range from 1 to 3 for enzyme reactions involving NAD(P)H oxidation (*24*). Thermodynamic and steady-state considerations have been offered to explain the lowered than expected values for primary deuterium isotope effects (*15*).

Another application of primary deuterium kinetic isotope effect analysis is to distinguish between kinetic mechanisms by evaluating the dependence of the apparent $^{D}V/K$ for one substrate on the concentration of the cosubstrate based on the mechanism-dependent magnitudes of the forward commitment factors[3] (*16*). Considering A and B as, respectively, the first and second substrate to bind to the enzyme, $^{D}V/K_A$ will decrease to unity when the concentration of B is raised to saturating levels, while $^{D}V/K_B$ will not change with varying concentrations of A, if the mechanism is steady-state-ordered. In the case where A and B can independently bind to the enzyme and the mechanism is steady-state-random, $^{D}V/K_A$ will decrease to a constant value greater than unity if the concentration of B is raised to saturating levels and A is sticky,[4] whereas $^{D}V/K_B$ will be independent of the concentration of A, if B is not sticky (*16*). The investigation of the kinetic mechanism of 1-deoxy-D-xylulose-5-phosphate isomeroreductase (*25*) is a recent example of the utilization of this

[3] The commitment factor for a substrate is defined as the ratio of the rate constant for the isotope-sensitive step the net rate constant of dissociation of this substrate from the complex capable of proceeding forward in the reaction path through a step that contains the isotope-sensitive one. A commitment factor is composed of both internal and external portions. The internal portion is kept unchanged when the dissociation rate constant for the varied substrate is brought to infinite. The external portion includes the partition ratio, with the dissociation rate constant for the varied substrate in the denominator. For a more extended definition, see ref *16*.

[4] A substrate is sticky if it reacts to give products as fast as or faster than it dissociates from the enzyme. The stickiness of a substrate depends upon the external part of its commitment: the larger the external commitment, the sticker the substrate (*16*, *23*).

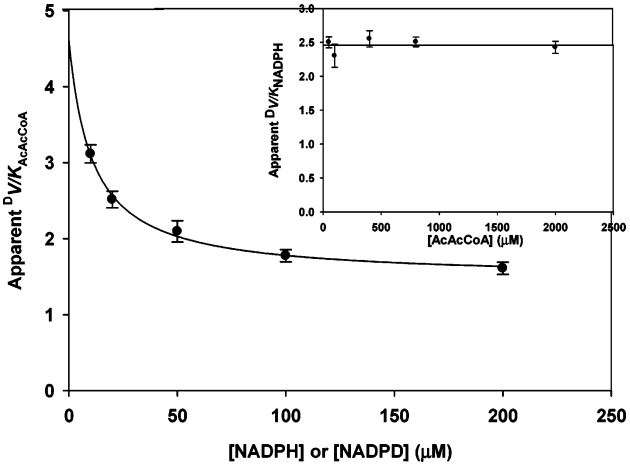

FIGURE 2: Dependence of the apparent $^{D}V/K_{AcAcCoA}$ values on the concentration of the cosubstrate. The data were fitted to an equation describing a hyperbolic decay, which yielded a limiting value of 1.6 ± 0.08 for $^{D}V/K_{AcAcCoA}$. The inset represents the independence of the $^{D}V/K_{NADPH}$ on the concentration of the cosubstrate.

Scheme 2: Proposed Kinetic Mechanism for *M. tuberculosis* β-Ketoacyl-ACP Reductase

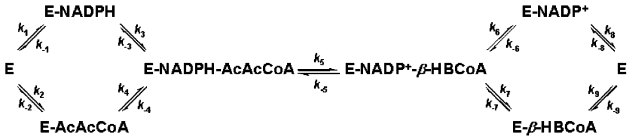

technique. In the present work, the apparent $^{D}V/K_{AcAcCoA}$ decreases to 1.6 ± 0.08 as the concentration of NADPH is raised to saturating levels (Figure 2), while $^{D}V/K_{NADPH}$ remains approximately 2.5 ± 0.09 at any concentration of AcAcCoA (inset in Figure 2). These results suggest a steady-state random mechanism for MabA, in agreement with the product inhibition patterns, and indicate that AcAcCoA is sticky. A random order of substrate binding was reported for the InhA enzyme based on primary deuterium isotope effects (*26*). Scheme 2 shows the proposed kinetic mechanism for MabA, where k_5 is a macroscopic rate constant containing the isotope-sensitive step. If substrate binding and dissociation are not in rapid equilibrium and AcAcCoA is sticky, the ratios k_5/k_{-3} and $k_5/(k_{-3} + k_{-4})$ represent the forward commitments for AcAcCoA when the NADPH concentration is saturating or very low, respectively, and are expected to possess finite values.

Solvent Isotope Effects and Proton Inventory. To examine the proton-transfer contribution to the rate of carbonyl reduction, solvent isotope effects were determined and are summarized in Table 2. No $^{D_2O}V/K_{AcAcCoA}$ was observed (Figure 3A). Solvent isotope effects on V (2.4) and V/K_{NADPH} (1.3) were observed (Figure 3B), which indicates that at least one protonation step partly limits the reaction rate. Proton transfer has also been proposed to partially limit the rate of the InhA-catalyzed reaction, because significant solvent isotope effects were observed (*26*). Interestingly, while for MabA $^{D_2O}V/K_{NADPH}$ is smaller than ^{D_2O}V (Table 2), in the case of InhA, the larger solvent isotope effect was expressed on V/K_{NADPH} (*26*), suggesting that proton transfer is kinetically important in different portions of the reactions catalyzed by these two enzymes. Solvent isotope effects significantly smaller than the primary ones were observed for *S. pneumoniae* FabG, and a mechanism with two distinct transition

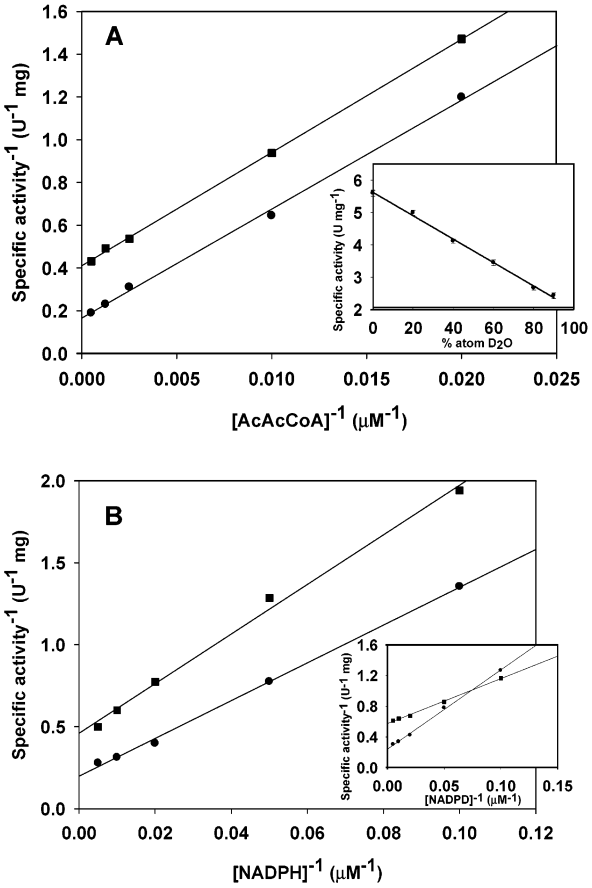

FIGURE 3: Solvent isotope effects for MabA. (A) AcAcCoA was used as the varied substrate, with a saturating concentration of the cosubstrate. The reaction mix contained either 0 (●) or 90 (■) atom % D_2O. The inset represents the proton inventory measured with both substrates at saturating concentrations. (B) NADPH was used as the varied substrate, with a saturating concentration of the cosubstrate. The inset shows the solvent isotope effect with NADPD as the varied substrate. The reaction mix contained either 0 (●) or 90 (■) atom % D_2O.

states were proposed, with the transition state for hydride transfer being rate-limiting (*17*). In the present work, primary and solvent isotope effects are nearly equivalent in magnitude, making the distinction between two transition states with different contributions to the reaction rate not clear. The stepwise addition of nucleophiles to carbonyl centers is not expected to proceed via a rate-limiting proton transfer, because it is generally characterized by a pre-equilibrium protonation step previous to nucleophilic attack or a diffusion-controlled protonation of the tetrahedral intermediate, depending upon which step comes first and the acidity of the proton-donating molecule. Accordingly, ^{D_2O}V values much larger than 1 are not characteristic of stepwise mechanisms, and the observation of a ^{D_2O}V value larger than or equal to 2, which indicates a contribution of proton transfer to the rate-determining step, as is seen here, is usually taken as evidence for a concerted mechanism (*27*).

In an attempt to assess the number of protons transferred during the solvent isotope-sensitive step, a proton inventory experiment was carried out. A linear relationship between V and the mole fraction of D_2O was obtained for MabA (inset in Figure 3A), suggesting that a single proton is transferred in the step that exhibits the solvent isotope effect (*28*). Similar

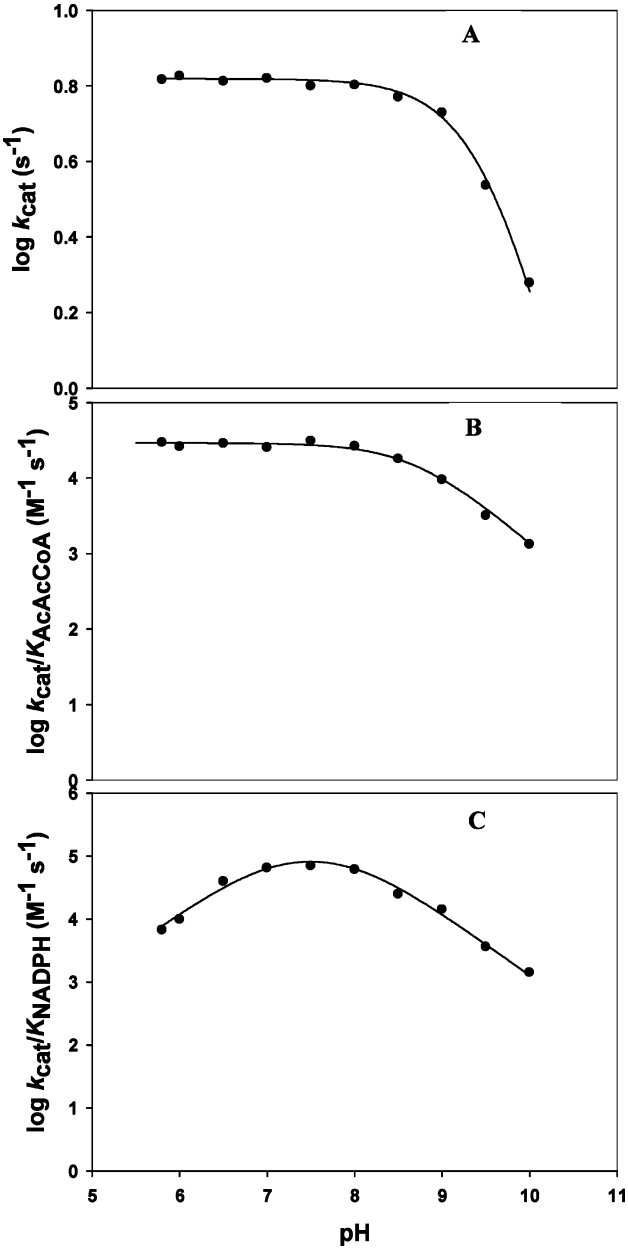

FIGURE 4: Dependence of kinetic parameters on pH. (A) pH dependence of log k_{cat}; the lines are fits to eq 4. (B) pH dependence of log $k_{cat}/K_{AcAcCoA}$; the lines are fits to eq 4. (C) pH dependence of k_{cat}/K_{NADPH}; the line is a fit to eq 5. The buffers utilized were PIPES (pH 5.8−6.0), HEPES (pH 6.5−8.5), and boric acid (pH 9.0−10).

proton inventory patterns have been observed for InhA[5] and for the *M. tuberculosis* NADPH-dependent mycothione reductase (*29*).

pH-Rate Profiles. To probe for acid−base catalysis, the pH dependence of kinetic parameters was determined. The pH-rate profiles are shown in Figure 4. The k_{cat} value is dependent upon a single enzyme group with a pK value of 9.6 ± 0.7, whose deprotonation abolishes activity (Figure 4A). This value lies in the normal pK range for phenol groups of tyrosine and ϵ-amino groups of lysine in proteins, and both of these residues have been proposed as part of the Ser-Tyr-Lys catalytic triad of the SDR family (*30*). Moreover, the phenol ring of Tyr153 rotates 90° and points into the

[5] Basso, L. A., and Blanchard, J. S. Unpublished data.

active site upon NADPH binding in MabA (*31*). Lys155 of *E. coli* FabG has been proposed to participate in the proton relay conduit proposed for this enzyme (*32*), suggesting that these residues play a critical role in catalysis and/or substrate binding. Hence, the group exhibiting the p*K* value reported is likely to be a component of the Ser-Tyr-Lys triad. The p*K* values for the active-site tyrosine in the SDR family have been suggested to be significantly lower than 9.6, because the interaction with the conserved active-site lysine would help to stabilize the conjugate base (*33*). Protonation of a group exhibiting a p*K* value of 8.3 seemed to be essential for the activity of the *S. pneumoniae* FabG, although fitting data to a more complex equation yielded a p*K* value of 9.4 (*17*).

The pH dependence of $k_{cat}/K_{AcAcCoA}$ (Figure 4B) indicates that deprotonation of a single group with an apparent p*K* value of 8.8 ± 0.5 abolishes the binding of the AcAcCoA substrate. It is likely that the ionization behavior of the same group is being observed in the pH profiles of *V* and *V*/*K* for AcAcCoA, and the difference in the p*K* values may reflect the perturbation of the p*K* value to a larger value upon substrate binding. A group with a p*K* value of 8.8 was also found to be important for substrate binding of the *S. pneumoniae* FabG enzyme (*17*). The data for the k_{cat}/K_{NADPH} profile was fitted to a bell-shaped curve (Figure 4C), with both deprotonation and protonation of groups with p*K* values of 6.9 ± 0.8 and 8.0 ± 0.6, respectively, being necessary for substrate binding. Values of 5.0 and 8.8 were reported for this profile with the *S. pneumoniae* enzyme (*17*). The value of 6.9 presented here is in agreement, within experimental error, with that reported for the 2′-phosphate group of NADPH (pK = 6.5), on the basis of NMR studies (*34*). Thus, it is possible that the group whose protonation decreases k_{cat}/K_{NADPH} is the 2′-phosphate moiety of NADPH. In summary, the data presented here for the pH profiles are slightly different from those previously reported for related enzymes, and site-directed mutagenesis experiments are currently underway to unambiguously assign the MabA residues playing a critical role in catalysis and substrate binding.

Temperature Effects. To determine the energy of activation of the MabA-catalyzed reaction, the temperature dependence of k_{cat} was analyzed. Fitting the data to eq 6 yielded a value of 9.0 kcal mol^{-1} for the activation energy. This value is very similar to that reported for the activation energy of the *M. tuberculosis* shikimate dehydrogenase-catalyzed reaction (8.5 kcal mol^{-1}), which is also an NADPH-dependent carbonyl reduction (*35*). In addition, the Arrhenius plot is linear (Figure 5), indicating that there is no change in the rate-limiting step over the temperature range utilized.

Regiospecificity of Hydride Transfer. To show the regiospecificity of the hydride transfer catalyzed by MabA, we used NADPH or [4*S*-4^{2}H]-NADPH and determined the position of transfer by ^{1}H NMR spectroscopy. The use of glucose dehydrogenase as a regenerating system drove the reaction to completion and minimized the amount of NADP$^+$ used, making the purification and analysis by NMR straightforward. As can be seen in Figure 6, the collapse of the resonance signals corresponding to the hydrogen atoms of C4 and C2, when the reaction was carried out with [4*S*-4^{2}H]-NADPH (top spectrum) compared to the identical reaction using NADPH, unambiguously indicates that the hydride is transferred to the C3 of the substrate. As expected, the reduction of C3 occurs directly and not through hydride transfer to C2 and protonation of C3.

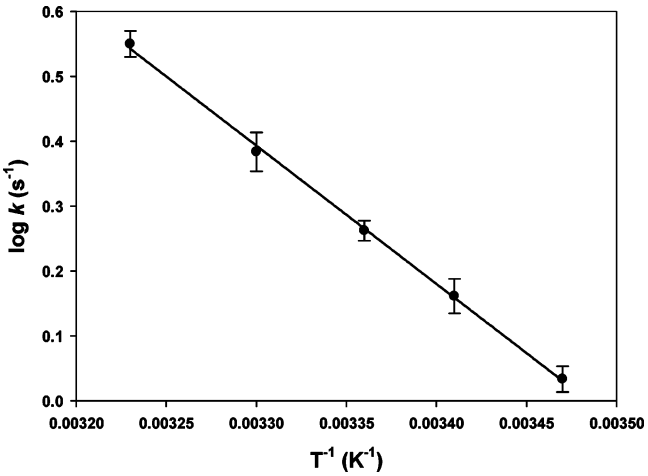

FIGURE 5: Temperature dependence of the log k_{cat}. Saturating conditions of substrates were determined and used at each temperature. The line is a fit to eq 6.

Multiple Isotope Effects and pH Variation of Primary Isotope Effects. Double isotope effect studies are able to distinguish whether two different isotopic substitutions affect the same or different chemical steps. Accordingly, with the intent of investigating whether MabA catalyzes the reduction of AcAcCoA in a concerted or stepwise fashion, solvent kinetic isotope effects were measured using either NADPH or NADPD as the varied substrate, and the results are reported in Table 2 and illustrated in the inset of Figure 3B. Assuming that the primary deuterium kinetic isotope effect is expressed only on the hydride transfer reaction and solvent isotope effects affect only the putative alkoxide protonation, deuteration of NADPH should slow the hydride transfer step. The theory predicts that, if protonation and hydride transfer occur in the same transition state, the solvent isotope effects will be larger or unchanged with NADPD as compared to NADPH. On the other hand, if hydride transfer and protonation occur in distinct steps, the solvent isotope effects will be smaller with NADPD as the substrate, because hydride transfer will become more rate-limiting (*36*, *37*). As can be seen in Table 2, the $^{D_2O}V/K_{NADPD}$ (0.58) decreased in comparison to $^{D_2O}V/K_{NADPH}$ (1.3), actually becoming inverse (inset of Figure 3B). While this result alone points to a stepwise mechanism, the $^{D_2O}V_{NADPD}$ was unchanged within experimental error, consistent with a concerted mechanism. As pointed out by Patel et al. (*17*), there is a possibility that, for the di-keto form of AcAcCoA, five protons exchange to deuterons when the reaction is carried out in D_2O. Each deuterium would be expected to contribute a β-secondary kinetic isotope effect of 0.96 (*38*), with a maximal value of 0.82 for all five deuterons, which might be contributing for the inverse $^{D_2O}V/K_{NADPD}$ observed here. A mixture of proton transfer and inverse equilibrium isotope effects may also be used to interpret some observed inverse solvent isotope effects, depending upon their magnitudes, provided that the equilibrium effects dominate (*39*). Because the multiple isotope effect on *V* is normal, whereas the effect on *V*/*K* is inverse, the solvent isotope effects for NADPD are likely to be reporting on two different steps of the reaction mechanism. The inverse multiple isotope effect on *V*/*K* may reflect

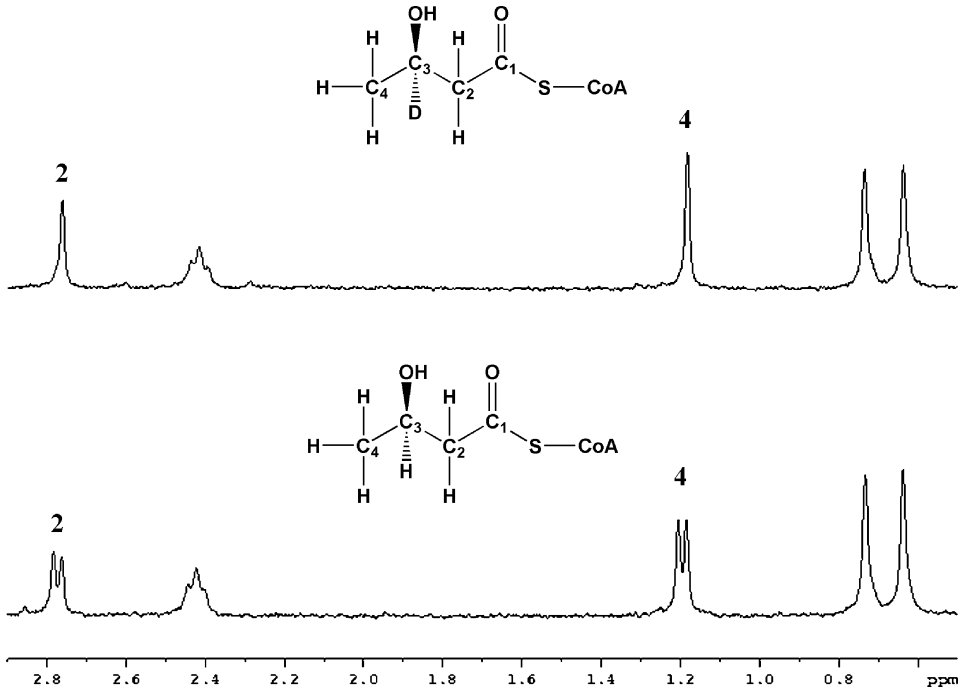

FIGURE 6: ^{1}H NMR spectra of the β-hydroxybutyryl-CoA produced by MabA. The reaction product was generated in the presence of NADPH (bottom) and NADPD (top). Resonances at ~2.45, 0.65, and 0.75 ppm are derived from the CoA moiety. The C3 hydrogen resonance was not observed directly because of overlap with a peak from CoA.

an inverse equilibrium isotope effect preceding chemistry. Inverse solvent kinetic isotope effects on V/K were also reported for InhA using dodecenoyl-CoA as the varied substrate (*26*). This result was explained on the basis of a possible inverse equilibrium isotope effect on a conformational change taking place simultaneous to or after dodecenoyl-CoA binding to the enzyme (*26*). If an analogous line of reasoning was followed here to account for the inverse $^{D_2O}V/K_{NADPD}$, supported by the fact that an enzyme conformational change upon NADPH binding was reported for MabA (*31*), one would be tempted to consider the possibility of different equilibrium isotope effects on this conformational change, in D_2O, when either NADPD or NADPH was employed as the substrate, because the $^{D_2O}V/K_{NADPH}$ was normal (Figure 3B). However, further experimental results are needed to confirm or discard this proposal.

Because multiple isotope effect analysis led to some mixed conclusions about the chemical mechanism of the MabA-catalyzed reaction, measurements of the primary isotope effects in a pH where the chemical step has become more rate-limiting were carried out to distinguish between concerted and stepwise mechanisms. Again, if both protonation and hydride transfer take place in the same step, both $^{D}V/K$ and ^{D}V will be either pH-independent or larger but should become equal (*40*). On the other hand, for a stepwise mechanism, the primary isotope effects will reduce to unity (in the direction where the pH-dependent step precedes the isotope-dependent one) or to the equilibrium isotope effect (in the direction where the isotope-dependent step precedes the pH-dependent one) (*40*). Accordingly, the primary isotope effects for MabA were determined at pH 10.0, with NADPH as the varied substrate, and the results are shown in Figure 7 and Table 2. The isotope effect on V/K was unchanged, while the isotope effect on V increased to 2.4, with both isotope effects becoming equal within experimental error, suggesting that hydride transfer and protonation occur in the same transition state, in agreement with the conclusions drawn from the results of multiple isotope effects on V and from the magnitude of $^{D_2O}V_{NADPH}$. The pH independence of

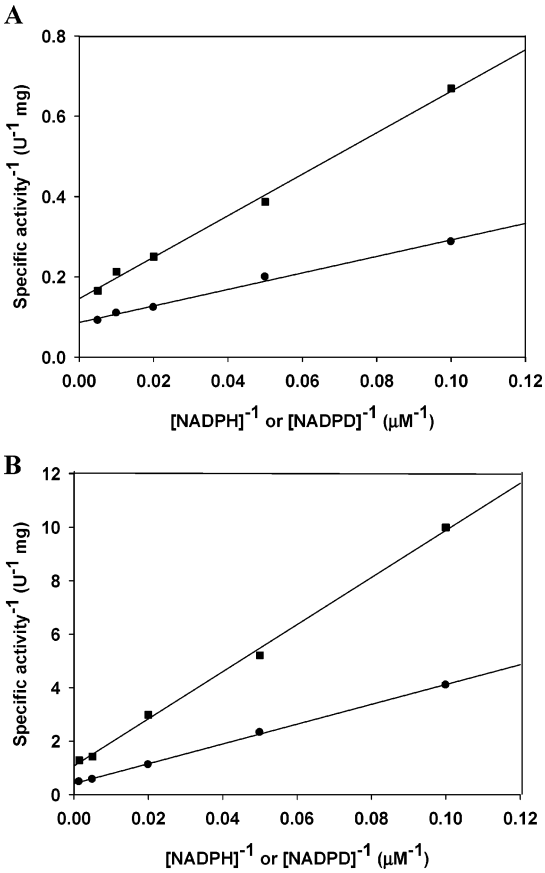

FIGURE 7: Dependence of primary isotope effects on pH. The primary kinetic isotope effects were determined in pH 7.0 (A) and pH 10.0 (B) with either NADPH (●) or NADPD (■) as the varied substrate, with a saturating concentration of cosubstrate.

Scheme 3: Proposed Chemical Mechanism for the β-Ketoacyl-ACP-Reductase-Catalyzed Reaction[a]

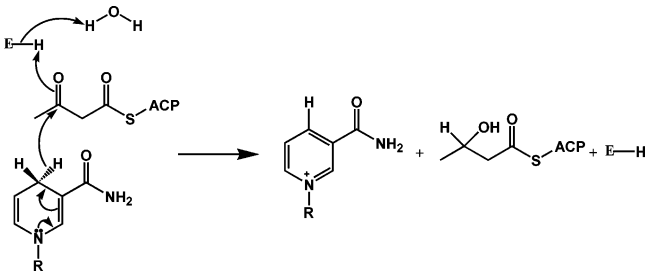

[a] R = ribose, adenosine diphosphate, and 2′-phosphate moieties of Nadph.

$^{D}V/K_{NADPH}$ further indicates that this substrate is not sticky. A chemical mechanism for the MabA-catalyzed reaction is proposed on the basis of these results (Scheme 3).

Enzymes often make use of concerted mechanisms to bypass unstable intermediates, such as some enolate anions (*42*, *43*). The β-elimination catalyzed by bovine liver crotonase is concerted (*44*), as well as the reactions catalyzed by pig liver acyl-CoA dehydrogenase (*45*) and isocitrate dehydrogenase (*40*). In contrast to the results observed here, hydride transfer is proposed to precede protonation in the reactions catalyzed by InhA and *S. pneumoniae* FabG (*17*, *26*). The case of MabA and *S. pneumoniae* FabG is an instance of enzymes from different sources that seem to have evolved to catalyze the same reaction through different mechanisms.

Summary. In the present work, MabA has been shown to catalyze the NADPH-dependent reduction of AcAcCoA by a steady-state random bi-bi kinetic mechanism, in which AcAcCoA is sticky, whereas NADPH is not. The magnitudes of the primary isotope effects indicated that the C_4-*proS* hydrogen is transferred to the acyl substrate and partly limits the reaction. Proton inventory and solvent isotope effects suggested that transfer of a single proton is also partly rate-limiting. In addition, hydride transfer and protonation were proposed to occur in the same step, according to the analysis of multiple isotope effects, pH variation of isotope effects, and the magnitude of $^{D_2O}V_{NADPH}$. Because the chemistry does not seem to be fully rate-limiting, steps other than the chemical ones should also be associated with an energy barrier of 9 kcal mol^{-1}. The hydride was shown, by NMR analysis, to be transferred to the C3 of AcAcCoA. The pH dependence of k_{cat} identified a general acid as being essential for catalysis. The pH dependence of k_{cat}/K_{NADPH} revealed the importance of the ionization state of the 2′-phosphate moiety of NADPH in binding. These results may be useful for the rational design of chemotherapeutic agents to treat TB.

ACKNOWLEDGMENT

We are grateful to Dr. William R. Jacobs, Jr. for his generous gift of a plasmid containing the *mabA* gene and to Dr. Paul F. Cook and Dr. Argyrides Argyrou for their insightful contributions to the analysis of pH variation of isotope effects. We also acknowledge Marcelo M. Pedroso for helpful discussions. This work is dedicated to a lifetime of achievement in academia by Tuiskon Dick.

REFERENCES

1. World Health Organization (2005) Surveillance, planning, financing, *WHO Report*, Geneva, Switzerland, WHO/HTM/TB/2005.349.
2. Sharma, S. K. (2004) Antituberculosis drugs and hepatotoxicity, *Infect. Genet. Evol. 4*, 167−170.
3. Stockstad, E. (2000) Drug-resistant TB on the rise, *Nature 287*, 2391.
4. Heath, R. J., White, S. W., and Rock, C. O. (2001) Lipid biosynthesis as a target for antibacterial agents, *Prog. Lipid Res. 40*, 467−497.
5. Schroeder, E. K., de Souza, O. N., Santos, D. S., Blanchard, J. S., and Basso, L. A. (2002) Drugs that inhibit mycolic acid biosynthesis in *Mycobacterium tuberculosis*, *Curr. Pharm. Biotechnol. 3*, 197−225.
6. Banerjee, A., Sugantino, M., Sacchettini, J. C., and Jacobs, W. R., Jr. (1998) The mabA gene from the inhA operon of *Mycobacterium tuberculosis* encodes a 3-ketoacyl reductase that fails to confer isoniazid resistance, *Microbiology 144*, 2697−2707.
7. Marrakchi, H., Ducasse, S., Labesse, G., Montrozier, H., Margeat, E., Emorine, L., Charpentier, X., Mamadou, D., and Quémard, A. (2002) MabA (FabG1), a *Mycobacterium tuberculosis* protein involved in the long-chain fatty acid elongation system FAS-II, *Microbiology 148*, 951−960.
8. Oppermann, U., Filling, C., Hult, M., Shafqat, N., Wu, X., Lindh, M., Shafqat, J., Nordling, E., Kallberg, Y., Persson, B., and Jörnval, H. (2003) Short-chain dehydrogenases/reductases (SDR): The 2002 update, *Chem.-Biol. Interact. 143*−*144*, 247−253.
9. Cohen-Gonsaud, M., Ducasse, S., Hoh, F., Zerbib, D., Labesse, G., and Quémard, A. (2002) Crystal structure of MabA from *Mycobacterium tuberculosis*, a reductase involved in long-chain fatty acid biosynthesis, *J. Mol. Biol. 320*, 249−261.
10. Ducasse-Cabanot, S., Cohen-Gonsaud, M., Marrakchi, H., Nguyen, M., Zerbib, D., Bernadou, J., Daffé, M., Labesse, G., and Quémard, A. (2004) In vitro inhibition of the *Mycobacterium tuberculosis* β-ketoacyl-acyl carrier protein reductase MabA by isoniazid, *Antimicrob. Agents Chemother. 48*, 242−249.
11. Laemmli, U. K. (1970) Cleavage of structural proteins during the assembly of the head of bacteriophage T4, *Nature 227*, 680−685.
12. Bradford, M. M., McRorie, R. A., and Williams, W. L. (1976) A rapid and sensitive method for the quantitation of microgram quantities of protein utilizing the principle of protein−dye binding, *Anal. Biochem. 72*, 248−254.
13. Ottolina, G., Riva, S., Carrea, G., Danieli, B., and Buckmann, A. F. (1989) Enzymatic synthesis of [4*R*-^{2}H]NAD(P)H and [4*S*-^{2}H]-NAD(P)H and determination of the stereospecificity of 7α- and 12α- hydroxysteroid dehydrogenase, *Biochim. Biophys. Acta 998*, 173−178.
14. Orr, G. A., and Blanchard, J. S. (1984) High-performance ion-exchange separation of oxidized and reduced nicotinamide adenine dinucleotides, *Anal. Biochem. 142*, 232−234.
15. Northrop, D. B. (1975) Steady-state analysis of kinetic isotope effects in enzymic reactions, *Biochemistry 14*, 2644−2651.
16. Cook, P. F., and Cleland, W. W. (1981) Mechanistic deductions from isotope effects in multireactant enzyme mechanisms, *Biochemistry 20*, 1790−1796.
17. Patel, M. P., Liu, W., West, J., Tew, D., Meek, T. D., and Thrall, S. H. (2005) Kinetic and chemical mechanisms of the fabG-encoded *Streptococcus pneumoniae* β-ketoacyl-ACP reductase, *Biochemistry 44*, 16753−16765.
18. Quémard, A., Sacchettini, J. C., Dessen, A., Vilcheze, C., Bittman, R., Jacobs, W. R., Jr., and Blanchard, J. S. (1995) Enzymatic characterization of the target for isoniazid in *Mycobacterium tuberculosis*, *Biochemistry 34*, 8235−8241.
19. Fawcett, T., Copse, C. L., Simon, W. J., Slabas, A. R. (2000) Kinetic mechanism of NADH-enoyl-ACP reductase from *Brassica napus*, *FEBS Lett. 484*, 65−68.
20. Segel, I. H. (1975) *Enzyme Kinetics. Behavior and Analysis of Rapid Equilibrium and Steady-State Enzyme Systems*, pp 646−656, John Wiley and Sons, Inc., New York.
21. Wickramasinghe, S. R., Inglis, K. A., Urch, J. E., Müller, S., van Aalten, D. M. F., and Fairlamb, A. H. (2006) Kinetic, inhibition and structural studies on 3-oxoacyl-ACP reductase from *Plasmodium falciparum*, a key enzyme in fatty acid biosynthesis, *Biochem. J. 393*, 447−457.
22. Price, A. C., Zhang, Y., Rock, C. O., White, S. W. (2001) Structure of β-ketoacyl-[acyl carrier protein] reductase from *Escherichia coli*: Negative cooperativity and its structural basis, *Biochemistry 40*, 12772−12781.

23. Schowen, K. B., and Schowen, R. L. (1981) The use of isotope effects to elucidate enzyme mechanisms, *BioScience 31*, 826−831.
24. Cook P. F. (1981) Kinetic and regulatory mechanisms of enzymes from isotope effects, in *Enzyme Mechanisms from Isotope Effects* (Cook, P. F., Ed.) pp 203−228, CRC Press, Boca Raton, FL.
25. Argyrou, A., and Blanchard, J. S. (2004) Kinetic and chemical mechanism of *Mycobacterium tuberculosis* 1-deoxy-D-xylulose-5-phosphate isomeroreductase, *Biochemistry 43*, 4375−4384.
26. Parikh, S., Moynihan, D. P., Xiao, G., and Tonge, P. (1999) Roles of tyrosine 158 and lysine 165 in the catalytic mechanism of InhA, the enoyl-ACP reductase from *Mycobacterium tuberculosis*, *Biochemistry 38*, 13623−12634.
27. Klinman, J. P. (1978) Kinetic isotope effects in enzymology, *Adv. Enzymol. Relat. Areas Mol. Biol. 46*, 415−494.
28. Quinn, D. M., and Sutton, L. D. (1991) Theoretical basis and mechanistic utility of solvent isotope effects, in *Enzyme Mechanism from Solvent Isotope Effects*, 1st ed. (Cook, P. F., Ed.) pp 73−126, CRC Press, Boca Raton, FL.
29. Patel, M. P., and Blanchard, J. S. (2001) *Mycobacterium tuberculosis* mycothione reductase: pH dependence of the kinetic parameters and kinetic isotope effects, *Biochemistry 40*, 5119−5126.
30. Jörnival, H., Persson, B., Krook, M., Atrian, S., Gonzàlez-Duarte, R., Jeffrey, J., and Ghosh, D. (1995) Short-chain dehydrogenases/reductases (SDR), *Biochemistry 34*, 6003−6013.
31. Cohen-Gonsaud, M., Ducasse-Cabanot, S., Quémard, A., and Labesse, G. (2005) Ligand-induced fit in mycobacterial MabA: The sequence-specific C-terminus locks the conformational change, *Proteins 60*, 392−400.
32. Price, A. C., Zhang, Y., Rock, C. O., and White, S. W. (2004) Cofactor-induced conformational rearrangements establish a catalytically competent active site and a proton relay conduit in FabG, *Structure 12*, 417−428.
33. Filling, C., Berndt, K. D., Benach, J., Knapps, S., Prozorovski, T., Nordling, R., Ladenstein, R., Jörnival, H., Oppermann, U. (2002) Critical residues for structure and catalysis in short-chain dehydrogenases/reductases, *J. Biol. Chem. 277*, 25677−25684.
34. Mas, M. T., and Colman, R. F. (1984) Phosphorus-31 nuclear magnetic resonance studies of the binding of nucleotides to $NADP^+$-specific isocitrate dehydrogenase, *Biochemistry 23*, 1675−1683.
35. Fonseca, I. O., Magalhães, M. L., Oliveira, J. S., Silva, R. G., Mendes, M. A., Palma, M. S., Santos, D. S., and Basso, L. A. (2005) Functional shikimate dehydrogenase from *Mycobacterium tuberculosis* H37Rv: Purification and characterization, *Protein Expression Purif.*, in press.
36. Hermes, J. D., Roeske, C. A., O'Leary, M. H., and Cleland, W. W. (1984) Use of multiple isotope effects to determine enzyme mechanisms and intrinsic isotope effects. Malic enzyme and glucose-6-phosphate dehydrogenase, *Biochemistry 21*, 5106−5114.
37. Belasco, J. G., Albery, J., and Knowles, J. R. (1983) Double isotope fractionation: Test for concertedness and for transition-state dominance, *J. Am. Chem. Soc. 105*, 2475−2477.
38. Geneste, P., Lamaty, G., and Roque, J. P. (1971) Reactions d'addition nucléophile sur les cétones: Addition de l'ion sulfite: Mise en evidence de l'hyperconjugaison par la mésure de l'éffet isotopique sécondaire du deuterium, *Tetrahedron 27*, 5539−5559.
39. Merkler, D. J., Kline, P. C., Weiss, P., and Schramm, V. L. (1993) Transition-state analysis of AMP deaminase, *Biochemistry 32*, 12993−13001.
40. Cook, P. F., and Cleland, W. W. (1981) pH variation of isotope effects in enzyme-catalyzed reactions. 1. Isotope- and pH-dependent steps the same, *Biochemistry 20*, 1797−1805.
41. Cook, P. F., and Cleland, W. W. (1981) pH variation of isotope effects in enzyme-catalyzed reactions. 2. Isotope-dependent step not pH-dependent. Kinetic mechanism of alcohol dehydrogenase, *Biochemistry 20*, 1805−1816.
42. Thibblin, A., and Jencks, W. P. (1979) Unstable carbanions. General acid catalysis of the cleavage of 1-phenylcyclopropanol and 1-phenyl-2-arylcyclopropanol anions, *J. Am. Chem. Soc. 101*, 4963−4973.
43. Gerlt, J. A. (1998) Understanding the mechanisms and rates of enzyme-catalyzed proton transfer reactions to and from carbon, in *Bioorganic Chemistry: Peptides and Proteins*, 1st ed. (Hetch, S. M., Ed.) pp 279−311, Oxford University Press, New York.
44. Bahnson, B. J., and Anderson, V. E. (1991) Crotonase-catalyzed β-elimination is concerted: A double isotope effect study, *Biochemistry 30*, 5894−5906.
45. Pohl, B., Raichle, T., and Ghisla, S. (1986) Studies on the reaction mechanism of general acyl-CoA dehydrogenase. Determination of selective isotope effects in the dehydrogenation of butyryl-CoA, *Eur. J. Biochem. 160*, 109−115.

BI0611210